The 5th International Symposium – Supercritical CO2 Power Cycles
March 28-31, 2016, San Antonio, Texas

Short Duration Corrosion Performance of Carbon Steels in S-CO_2 at 260°C

M.S. Walker, A.M. Kruizenga, E.A. Withey, D. D. Fleming, J. J. Pasch
Sandia National Laboratories
Livermore, CA USA

Dr. Matthew Walker (mswalke@sandia.gov) is a Senior Member of the Technical Staff at Sandia National Laboratories California. He specializes in the interaction of materials with their environment and with other materials at high temperature. His current research interest is focused on the evaluation of structural alloys for use in advanced energy systems. Most prominent among these are evaluating alloy performance in supercritical CO_2, which cuts across a range of energy technologies including nuclear, fossil, as well as renewable. Prior to joining Sandia, he worked for 5 years as a Materials Scientist at the Alcoa research center in Pittsburgh, PA. While at Alcoa, he developed ceramic and metallic materials for operation within the aggressive environments of molten fluoride salt as well as in molten aluminum. Before joining Alcoa, he received a MS and PhD in Materials Science and Engineering at Carnegie Mellon University.

Dr. Alan Kruizenga (MS Nuclear Engineering and Engineering Physics (NEEP) '07, MS Mechanical Engineering and PhD NEEP '10) is a Principal Member of the Technical Staff at Sandia National Laboratories California, where he currently leads work investigating materials compatibility, materials selection, and efficiency-generating technology for solar power systems and advanced reactor concepts. Dr. Kruizenga is passionate about bringing practical knowledge, application-orientation, and problem-solving to theoretical science to make great ideas a reality. During his postgraduate studies at the University of Wisconsin - Madison, Dr. Kruizenga was a Nuclear Regulatory Fellow at the University of Wisconsin-Madison where his work focused on heat transfer in complex geometries for S-CO2 Brayton cycle application.

Dr. Elizabeth Withey (MS and PhD Materials Science and Engineering 2007 and 2009) is a postdoctoral appointee at Sandia National Laboratories, California currently characterizing materials interfaces used in energy generating technology. Dr. Withey avidly applies her materials science knowledge and practical characterization skills to help solve real-world materials problems. In her previous postdoctoral position at Lawrence Livermore National Laboratory, she investigated the use of metallic thin films in diffusion welding between dissimilar metals. During graduate school at the University of California, Berkeley, Dr. Withey probed the limits of strength and mechanisms for deformation in compression of nanopillars in a transmission electron microscope.

Mr. Darryn Fleming is a Senior Member of Technical Staff focused on engineering large scale experiments ranging from 20 MWth steam test facilities to highly complex S-CO2 power conversion cycles. Mr. Fleming is the Principal Investigator on several projects pertaining to the development of Supercritical CO2 power cycles which include scaling studies to reach a 10 MW unit along with US manufactured and US exportable advanced Printed Circuit Heat Exchangers.

Dr. Jim Pasch has professional experience in four distinct fields. In 1995, he supported the Air Force Air Combat Training Systems program as a systems engineer in Fort Walton Beach, Florida. In 1998, Pratt & Whitney hired Jim as a member of their rocket propulsion systems team in West Palm Beach, Florida. Jim spent eight years in this capacity analyzing test and flight data from the Space Shuttle Main Engine. Jacobs Engineering hired Jim in 2006 as NASA ramped up the Constellation program to replace the aging shuttle fleet. While working at Marshall Space Flight Center, Jim was tasked with analyzing and quantifying various thermal hydraulic and control risks to the successful launch of the Ares I-X mission. In 2010, Sandia National Labs hired Jim for his thermodynamic and thermal hydraulic expertise, first to support the nuclear waste disposal program in Carlsbad, New Mexico, then to take over as the principal investigator for Sandia closed Brayton cycle R&D efforts in Albuquerque.

ABSTRACT

The supercritical carbon dioxide (S-CO2) Brayton Cycle has gained significant attention in the last decade as an advanced power cycle capable of achieving high efficiency power conversion. Using carbon dioxide as the working fluid this cycle spans temperatures from ambient temperatures to >550°C. Low to intermediate temperatures may allow the use of carbon steel near the compressor. The power piping code, ASME B31.1, has stress levels for several carbon steels up to 426°C. This work investigates the corrosion rate of a seamless code qualified carbon steel (X65Q) that satisfies three of the specifications (A53, A106, and API-5L) within the ASTM Power Piping Code 31.1. Tests mimic intermediate conditions in Sandia's Closed S-CO_2 Brayton loop, 260°C at 17.6 MPa, with exposure durations ranging up to 2000 hours. Using conditions relevant to a commercial system, industrial grade CO_2 with a purity of 99.5% was utilized during these tests. Results indicate that this alloy demonstrates breakaway oxidation behavior after an exposure period of 1500 hrs. The post-breakaway corrosion rate was measured to be 0.032 mm/year. Corresponding to the onset of breakaway oxidation are cracks in the surface oxide along with oxide growth dominated by the magnetite inner oxide layer of the two layer (hematite + magnetite) corrosion products.

1. INTRODUCTION

Supercritical carbon dioxide (S-CO_2) closed Brayton cycles have been proposed for nuclear, concentrating solar, fossil energy, and heat recovery power generation applications. For these systems, the main advantages over the current steam plants are higher thermal efficiencies and reduced capital cost through extremely compact turbomachinery. Before the benefits of these systems can be realized, the underpinning technologies must be demonstrated to be ready and reliable. Sandia National Laboratories and the U.S. Department of Energy Office of Nuclear Energy (US DOE-NE) have been conducting research and development in order to deliver a technology that is ready for commercialization. Ongoing activities in support of this mission include: confirming the viability of existing components (bearing and gas seals) and suitability of materials, accommodating a wide range of operating parameters, integration and scale up of existing technologies into this new application, and developing robust operating procedures for operating at the critical point.

Integral to this mission is Sandia's S-CO_2 recompression closed Brayton cycle (RCBC) test loop facility, which is among the first and only of its kind in the world. At around 250kW_e in size, this test loop is utilized to investigate the key areas of technological uncertainty for this power cycle, and to confirm model estimates of advantageous thermodynamic performance. A recent photograph of the loop is shown in Fig. 1.

Developing a system with satisfactory capital costs is critical to the success of this mission. Heat exchangers play a critical role in S-CO_2 Closed Brayton Cycles (CBC), as significant recuperation in addition to the heat input and removal are required in order to achieve the high efficiencies associated with the proposed cycles [1], yet these are also expected to be the largest components in any S-CO_2 CBC, resulting in a significant portion of the overall cycle costs [2]. It is estimated that heat exchangers alone account for 40% of the Sandia RCBC test loop total capital costs. There is interest in identifying opportunities for balance of plant cost optimization. One possibility for this is a shift to more inexpensive alloys for the lower temperature portions of the system. The system temperatures range from room temperature up to 565^oC. While more expensive alloys (stainless steels and super alloys) are necessary for the higher temperature portions of the system, it may be possible to introduce inexpensive carbon steel into the lower temperature portions of the loop as a replacement for 316 stainless steel.

Corrosion experiments in S-CO_2 have focused predominantly on the expensive alloys for the aggressive (in terms of temperature and pressure) portions of these systems. Experimental data for inexpensive carbon steel alloys in this environment are sparse, while the impact of CO_2 corrosion on carbon steel has been studied extensively at pressures relevant for oil and gas transport (up to 2 MPa)[3]. The best information that exists relating to the performance of carbon steel in more relevant CO_2 environments comes from work done as part of the British MAGNOX and AGR nuclear reactor programs[4-9]. Much of this work was focused on understanding mechanisms for the breakaway oxidation that was observed under conditions relevant to these reactors. It appears that carbon steel is often susceptible to this enhanced form of attack in high pressure CO_2 environments at 350 – 500^oC. With regards to the corrosion rate in a relevant S-CO_2 environment, there was some work done at Idaho National Laboratory where they report a corrosion rate of 0.01 mm/year for iron over a period of approximately 5000 hrs at 162-183^oC and 8.7 – 12.3 MPa [10].

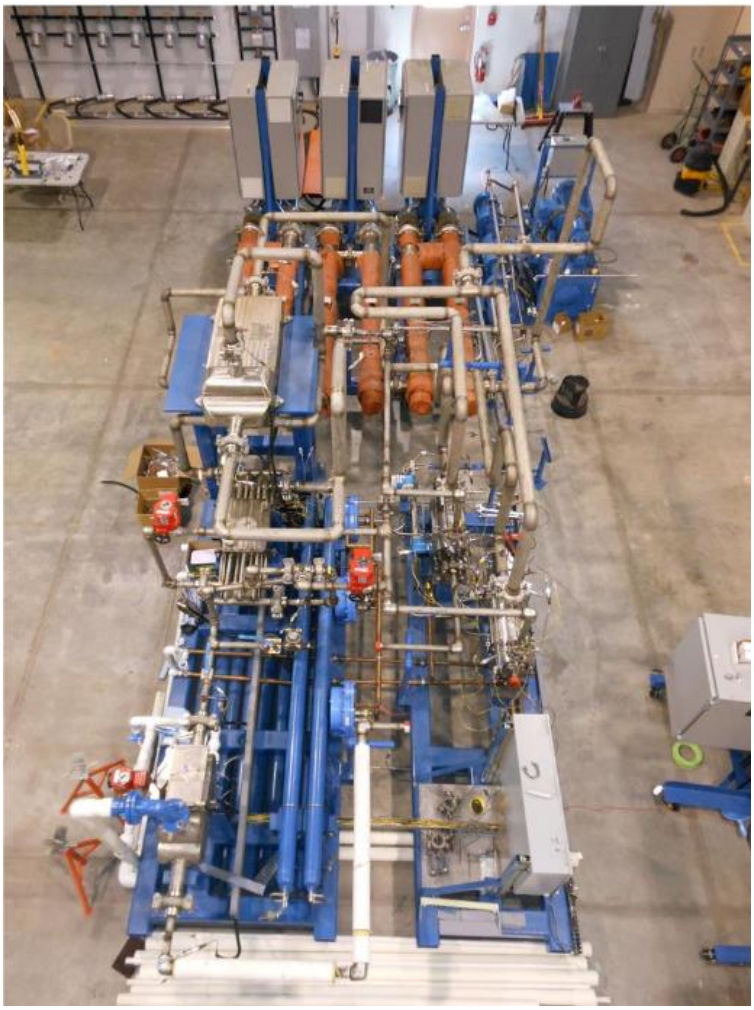

Fig. 1 Photograph of the Sandia S-CO_2 Brayton loop

In this paper, the corrosion performance of a mild carbon steel alloy (X65Q) was evaluated in S-CO_2 at 263^{o}C and 17.6 MPa, for exposure durations up to 2000 hours. The X65Q alloy was selected for this work as it is an alloy which satisfies three of the specifications (A53, A106, and API-5L) within the ASTM Power Piping Code 31.1.

2. EXPERIMENTAL PROCEDURE

2.1. Corrosion tests

The nominal composition of X65Q steel is listed in Table 1. The test samples were 32 mm diameter disks with a thickness of 1.5 mm. The samples were ground to 120 grit surface finish to replicate the surface finish of actual components. The specimens were ultrasonically cleaned in ethanol and acetone prior to exposure and suspended from an alumina rod with alumina spacers between individual specimens. A photograph of the sample holder is shown in Fig. 2. The samples were tested for a total exposure duration of 2000 hours, with samples being removed at intervals of 500 hours for analysis. Six samples were removed for analysis at each time interval.

Table 1
Element compositions (wt.%) in X65Q.

Fe	C	Mn	P	S	Si	Cu	Ni	Cr	Mo	Al	V	B	Ti	Nb
Bal	0.15	0.97	0.012	0.003	0.18	0.09	0.05	0.07	0.11	0.31	0.034	0.0003	0.003	0.002

Fig. 2. Photograph of the Inconel 625/Alumina sample holder

The S-CO_2 corrosion test facility that was developed at Sandia National Laboratories for these experiments utilizes an autoclave fabricated from Inconel 625 within a two-zone heated furnace. The autoclave has interior dimensions of 51 mm diameter by 610 mm length, and is rated to 650^{o}C at 31 MPa. A photograph of the corrosion test setup is shown in Fig. 3.

Industrial grade CO_2 with a purity of 99.5% was fed in a liquid state from a commercial cylinder (~ 5.7 MPa / 830 psi) to a Supercritical 24 constant flow dual piston pump, which subsequently supplied S-CO_2 to the autoclave chamber. A pressure transducer installed between this pump and the autoclave chamber is used to monitor pressure; S-CO_2 flow out from the pump is adjusted to provide the target chamber pressure as measured by this transducer. Autoclave temperature is measured using three thermocouples across the chamber length. A schematic of the autoclave chamber is shown Fig. 4, which points out the locations for these three thermocouples. Throughout this experiment the system was controlled to provide a pressure of 17.6 ± 0.2 MPa and a temperature of 263 ± 3^{o}C.

Fig. 3. Photograph of the Sandia S-CO_2 corrosion test facility

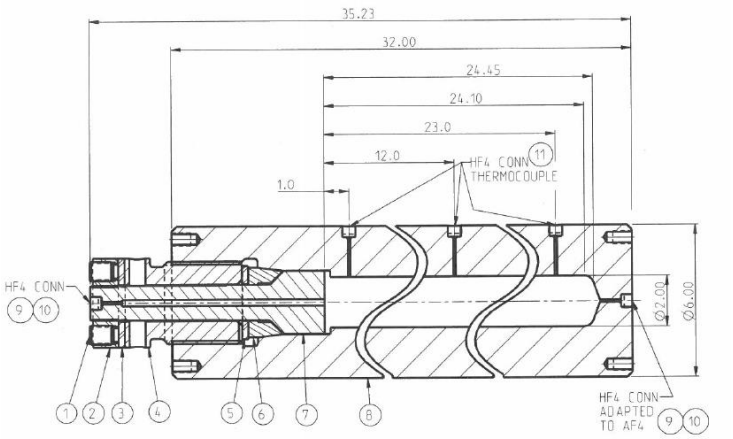

Fig. 4. Schematic of the Inconel 625 S-CO2 autoclave chamber

Two methods were used for evaluating the extent of sample corrosion. One method was to measure the sample weight gain as a function of test exposure time. For this, mass change due to corrosion was measured on an A&D model GH-252 balance (± 0.03 mg accuracy). While this method provides an indication of oxidation rate (rate of sample oxygen pickup through oxidation), it is difficult to extract a corrosion rate from this that could be used for making material lifetime predictions.

The second method enables lifetime predictions through the chemical removal of corrosion products from the samples, providing data for unaffected remaining metal as a function of exposure time. Three chemical descale treatments were selected from the ASTM Standard Practice for Preparing, Cleaning, and Evaluating Corrosion Test Specimens [11] and evaluated as part of this work. The three solutions used are listed in Table 2. Using samples from the first time interval, 500 hours exposure, each of the three solutions was evaluated; six descale cycles of 10 minutes each were used for this. The descale weight loss data for the three solutions is shown in Fig. 5. While each of the solutions was effective at removing the sample corrosion products, two of the solutions (Diammonium Citrate and HCl) exhibited extensive attack of the base metal. Based on this evaluation, the HCl-Hexamine solution was selected as the optimum solution to use for this study.

Table 2
Solutions evaluated for chemical descale of sample corrosion products.

Solution	Solution Temp (^{o}C)	Cycles	Cycle Duration (min)
6M HCl (21 wt %)	20-25	6	10
6M HCl (21 wt %) + Hexamethylene tetramine (0.3 wt %)	20-25	6	10
Diammonium Citrate (20 wt %)	75-90	6	10

Using the HCl-Hexamine solution, descale weight loss data for samples at each of the time intervals are shown in Fig. 6. It appears from this data that one 10 minute cleaning cycle is adequate for removing the corrosion products for samples with up to 2000 hours exposure; additional cleaning cycles appear to remove the base metal. For each exposure time, the descale weight loss after the first cleaning cycle is representative of its extent of corrosion. In this way, corrosion rate can be calculated for each time interval, incorporating this mass loss into Equation (1) below. The surface area for each sample was precisely measured prior to the experiment. An alloy density of 7.85 g/cm^3 is used for these calculations; this is the density for mild steel.

For the six samples extracted at each time interval, weight gain was measured for all six samples. Three of the six samples were subjected to the HCl-Hexamine descale treatment for weight loss measurements. The other three samples were utilized for microstructural and surface chemistry characterization.

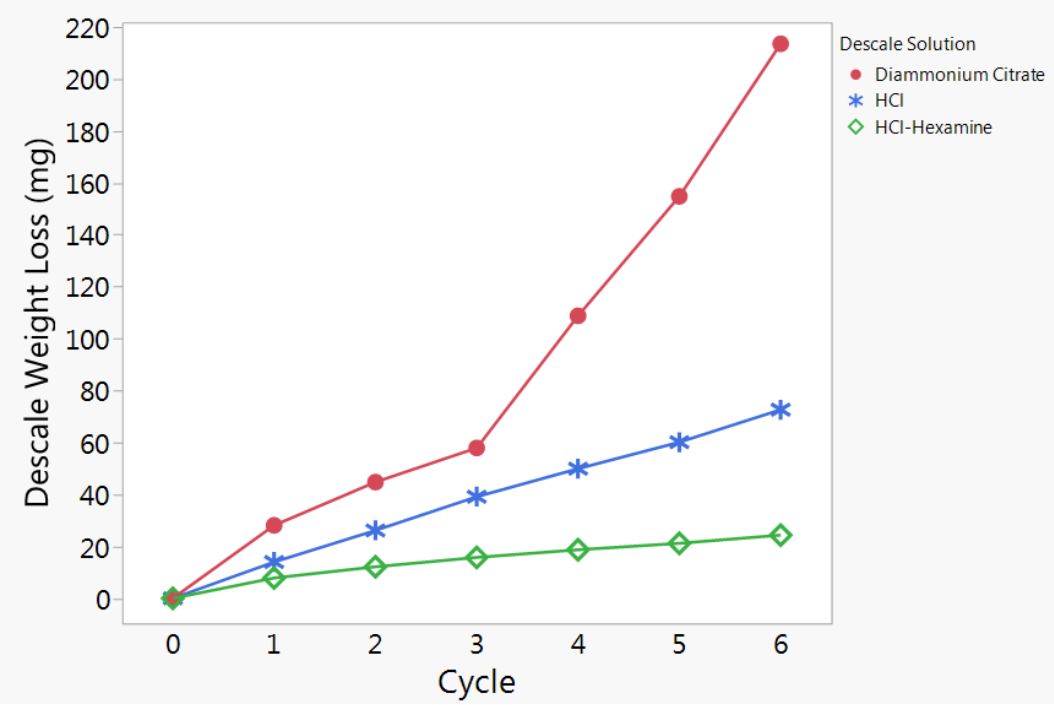

Fig. 5. Sample descale weight loss compared for three chemical solutions over 6 descale cycles

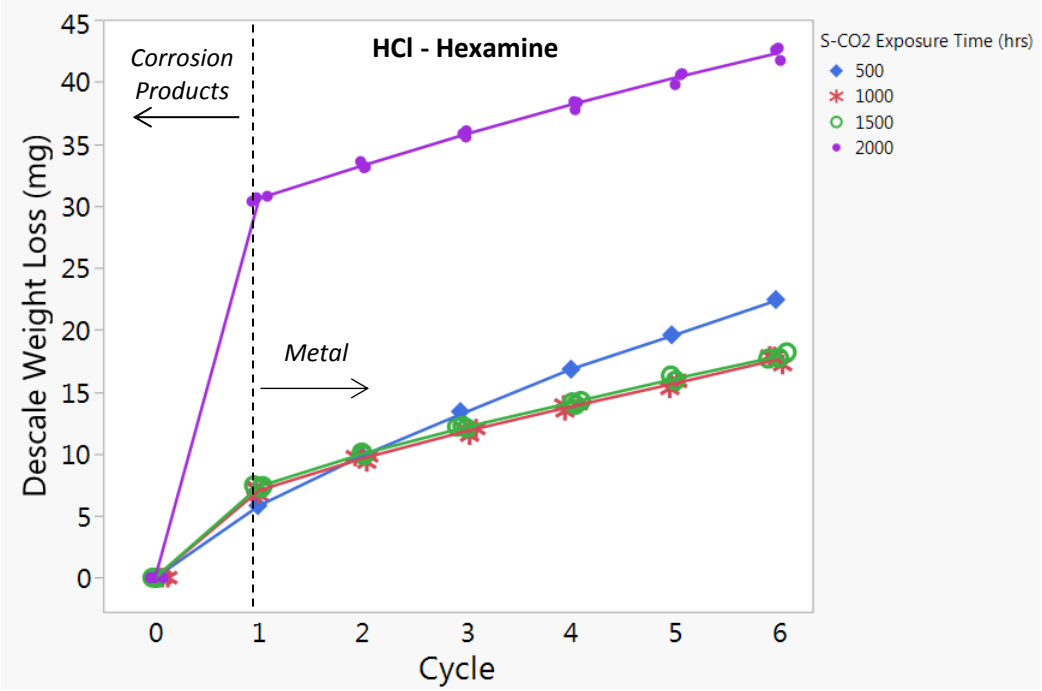

Fig. 6. Sample descale weight loss compared across the different S-CO2 exposure times

$$Corrosion\ Rate\ (mm/y) = \frac{8.76x10^4 * Mass\ Loss\ (g)}{Area\ (cm^2) * Alloy\ Density\ (g/cm^3) * Time\ (hrs)} \quad (1)$$

2.2. Microstructural characterization

Low magnification surface oxide morphology analysis was performed with a Keyence VHX-2000 optical microscope. Detailed images of the surface oxide were obtained using an FEI Phenom tabletop scanning electron microscope (SEM). Cross-sectional samples were prepared in an FEI Helios 660 Nanolab focused ion beam (FIB). Prior to extracting cross-sectional lamellae a carbon coating was deposited to protect the oxide surface. Thin lamellae were milled from 500- and 2000-hr samples using a standard in-situ lift-out method for transmission electron microscopy (TEM) samples. Imaging of the oxide layers was accomplished via the scanning transmission electron microscopy (STEM) mode in the FIB using bright field and high-angle-annular-dark-field (HAADF) detectors. Oxide thicknesses were measured directly from the HAADF images.

2.3. Surface characterization

Several different complimentary techniques were used to identify the chemistry of the corrosion products formed on the samples in S-CO_2. These are important as several different phases of iron oxide may form on carbon steel. The three techniques used for corrosion product chemistry include X-ray photoelectron spectroscopy (XPS), Raman spectroscopy, and X-ray diffraction (XRD).

For XPS characterization, spectra were obtained with an Al Kα source (Omicron model DAR400) using photons of 1490 eV. Photoelectrons were detected using a Physical Electronics model 10-360 electron energy analyzer. XPS was calibrated by adjusting the binding energy of the most prominent C 1s peak to 284.8 eV. The spectra were processed by the CasaXPS software using a Shirley-type background subtraction.

Raman spectroscopy was performed using a Renishaw InVia Micro-Raman spectrometer in air using a backscattering geometry with a 50X objective lens, a frequency-doubled Nd:YAG laser, and a CCD detector. The images scan used a step size of 0.5 μm.

XRD was performed using a PANalytical Empyrean unit. Using Copper Kα as the x-ray source, scans were conducted from 10 to 100 degrees 2θ ($^{o}2\theta$) with a step size of 0.013 $^{o}2\theta$. A scan step time of 129 seconds was use for these analyses. HighScore software was used for identifying chemical phases of the obtained diffraction patterns [12].

3. RESULTS

3.1. Corrosion measurements

The weight gain data for samples after exposure to S-CO_2 for every 500 hours up to 2000 hours is shown in Fig. 7. Six samples were measured at each 500 hour time interval. The values plotted are the average weight gain values. Error bars are included to indicate the range of weight gain among each set of samples. The rate of weight gain (i.e. oxidation) levels off starting around 1000 hours indicating that the oxide scale, which forms on the alloy, becomes protective after this initial exposure period. Starting around 1500 hours exposure, the oxide scale appears to lose its protective capability, as the rate of weight gain rapidly increases. The rapid increase in corrosion rate is indicative of breakaway corrosion; for this particular alloy the time to breakaway corrosion is 1500 hours.

For samples with S-CO_2 exposure up to 2000 hours, the sample weight loss after one chemical descale cycle is shown in Fig. 8. Again, average weight loss values are plotted. Three samples were measured at each 500 hour time interval, and error bars are included to indicate the range of weight loss among each set of samples. These sample weight loss values are consistent with the sample weight gain measurements, as the same trends in the data were observed.

The sample weight loss data can be used to calculate the corrosion rate for this particular alloy under the conditions of this test. Due to breakaway oxidation being observed for these samples, it is most useful to calculate the post-breakaway corrosion rate. In this way, the corrosion rate is calculated using Equation (1) along with the post-breakaway rate of sample weight loss from Fig. 8 (slope of line between 1500 and 2000 hours S-CO_2 exposure). This gives an average sample corrosion rate of 0.032 mm/year (1.25 mils/year).

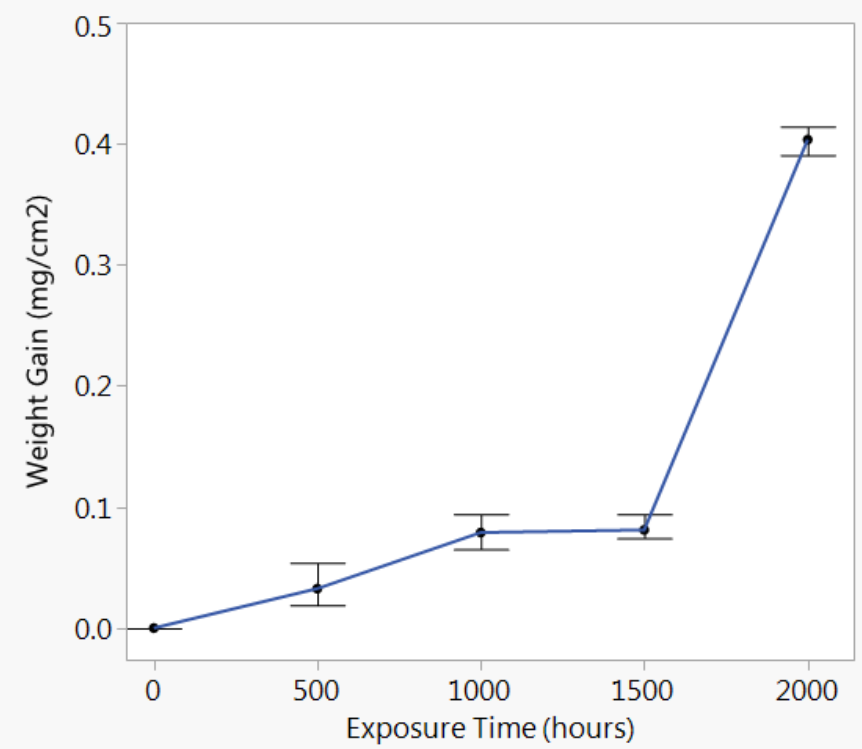

Fig. 7. Weight gain due to corrosion after exposure to S-CO_2 from 500 to 2000 hours

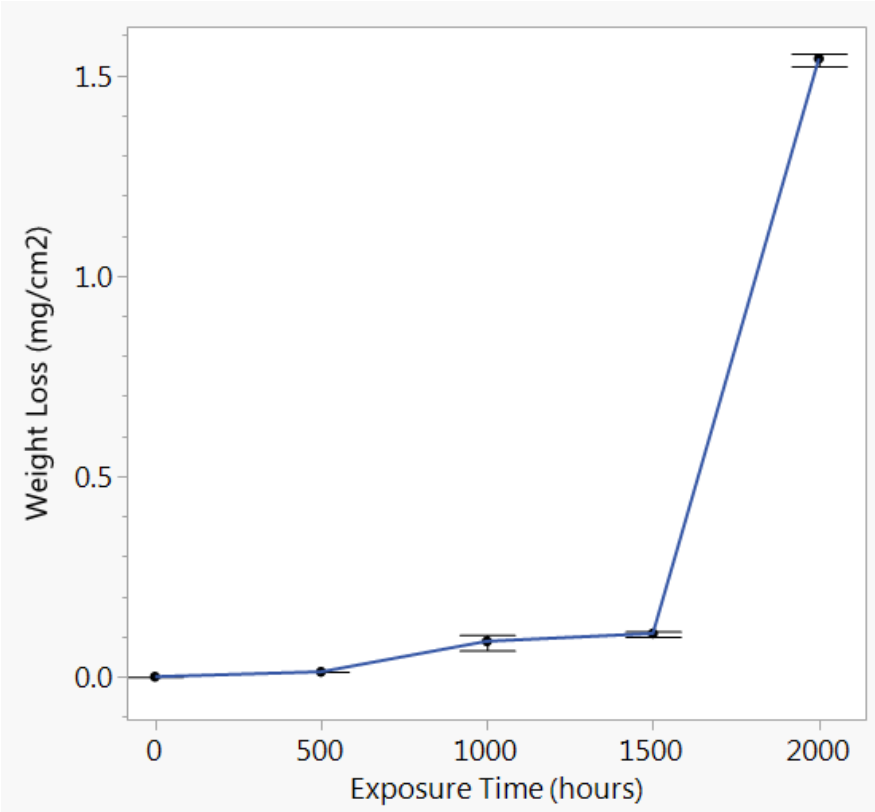

Fig. 8. Weight loss of corroded samples resulting from once chemical descale cycle

3.2. Microstructural characterization

Optical micrographs of representative samples from 500, 1000, 1500, and 2000 hour treatment increments are shown in the left column of Fig. 9. The samples darken in color with increasing exposure time up to 1000 hours with little change at longer exposure duration. It is assumed that the lighter non-uniform color of the 500 hour samples is indicative of incomplete coverage of the surface by oxide. With increasing time, the SEM micrographs in the right two columns of Fig. 9 indicate an increasing amount of surface oxide growth. Also, while islands of surface oxide appear on the sample surfaces, oxide is also present to varying degrees along the entire surface. At 2000 hours, this surface oxide shows distinct cracks which correlate with the breakaway portions of the weight gain/loss curves.

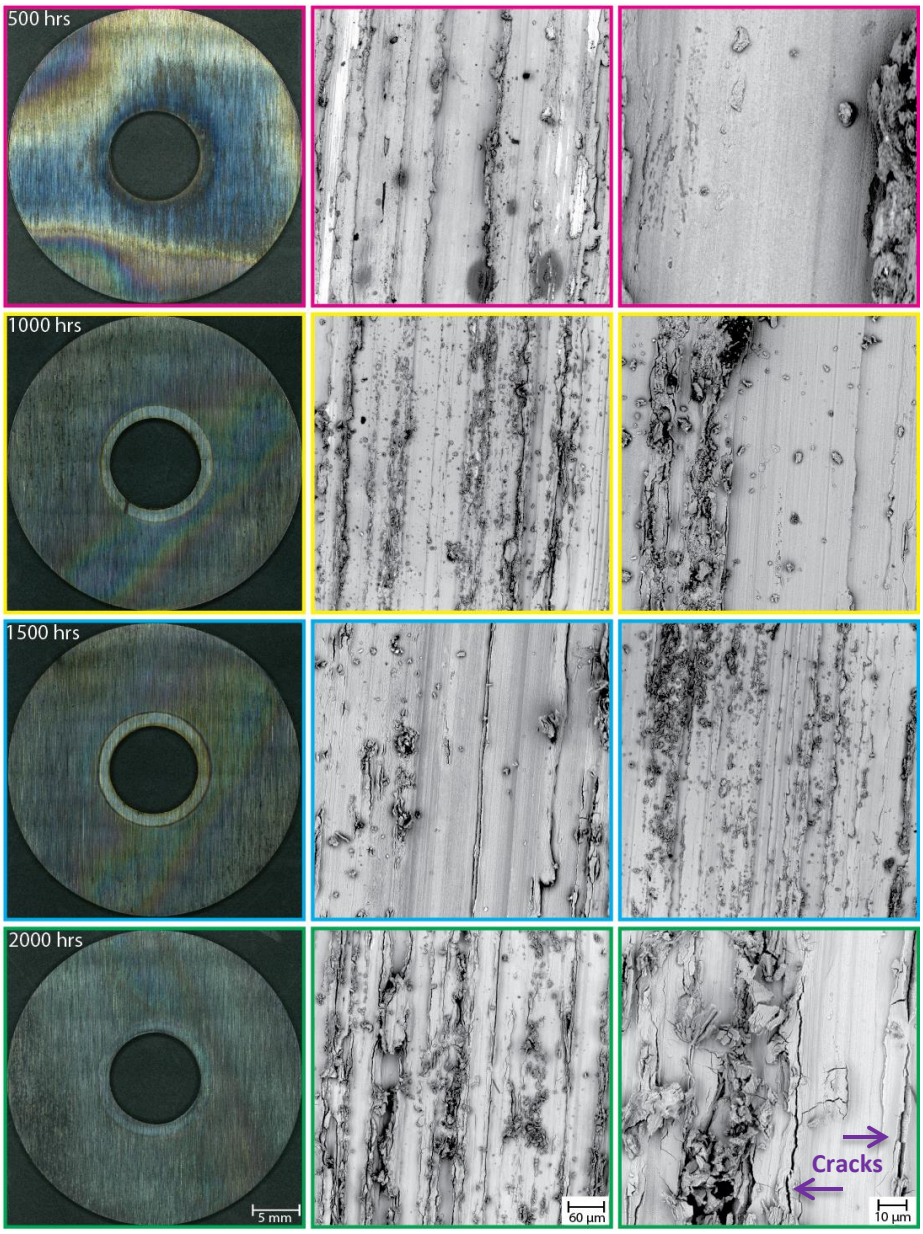

Fig. 9. Optical micrographs (left column) and SEM images taken at 500X (middle column) and 2400X (right column) magnifications.

Images from the FIB cross-section samples are shown in Fig. 10. The locations of the thinned lamellae, shown in the right two columns, are indicated by the arrows and labels in the left most column. Samples were extracted from areas of different surface topography; this includes raised areas or peaks as well as lower areas or valleys. This topography, with periodic waviness, is believed to result from the starting surface roughness of the samples. In both samples, the oxide layer is thicker on the peaks (B and D) than the valley areas (A and C). Multiple oxide layers are evident in regions where the oxide is thick; it is possible to designate these as three distinct layers. On the peak areas of both samples, and the valley area of the 2000-hr sample, the top oxide layer is ~ 25-70 nm thick followed by an intermediate layer that is up to 500 nm thick. The thickness of the oxide layer closest to the base metal (bottom layer) varies greatly between the two samples and is location dependent. At 500 hours, the intermediate and bottom oxide layers are not observed in the valley region. However, three distinct oxide layers are observed along the peak areas of the 500 hr sample and in both areas of the 2000 hr sample. The bottom layer increases in thickness from 500 nm along the peak area of the 500 hr sample to over 3 µm in the 2000 hr sample. This layer also appears to be denser in the 2000-hr sample. It should be noted that the color of the bottom oxide layer is darker than those nearer to the surface.

In Fig. 11 the measured oxide layer thicknesses are compared between samples at the two S-CO_2 exposure times. Here, the thicknesses are shown for the three distinct layers observed, and this is shown for both the peak and valley areas along the sample surfaces. This plot reveals that the large increase in overall oxide thickness going from 500 hrs to 2000 hrs is dominated by growth of the bottom-most oxide layer that sits next to the base metal. It is reasonable to associate the growth of this bottom oxide layer to the breakaway portion of the weight gain/loss curves.

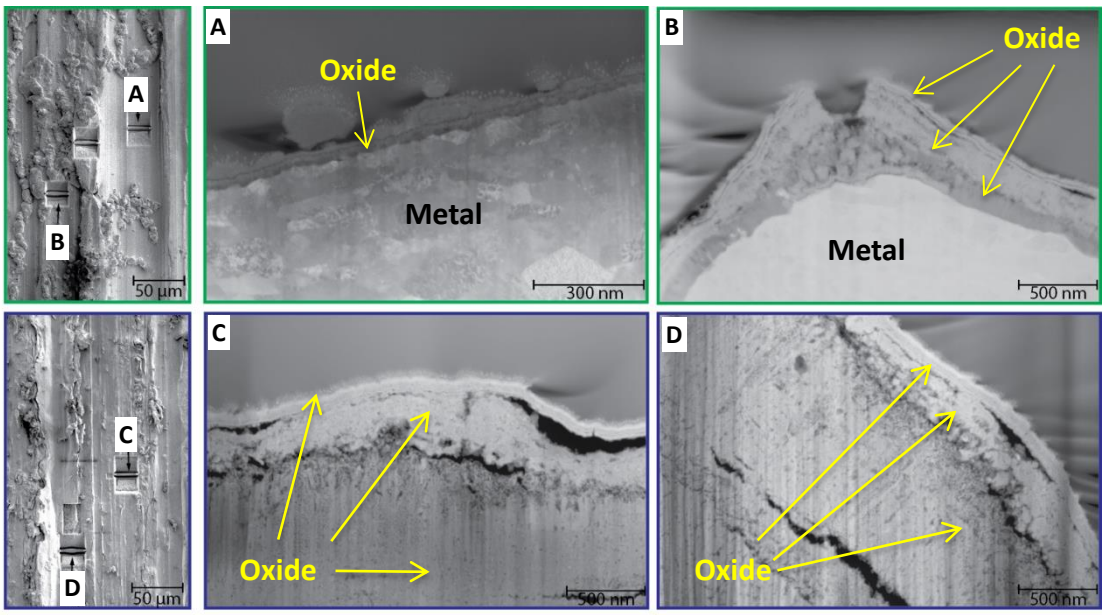

Fig. 10. SEM overview of sample surface in FIB indicating the location of lift out samples (left column and STEM HAADF images of thinned lamellae in flat (middle column) and raised (right column) areas. The 500 hour sample is shown in the top row and the 2000 hr sample in the bottom row.

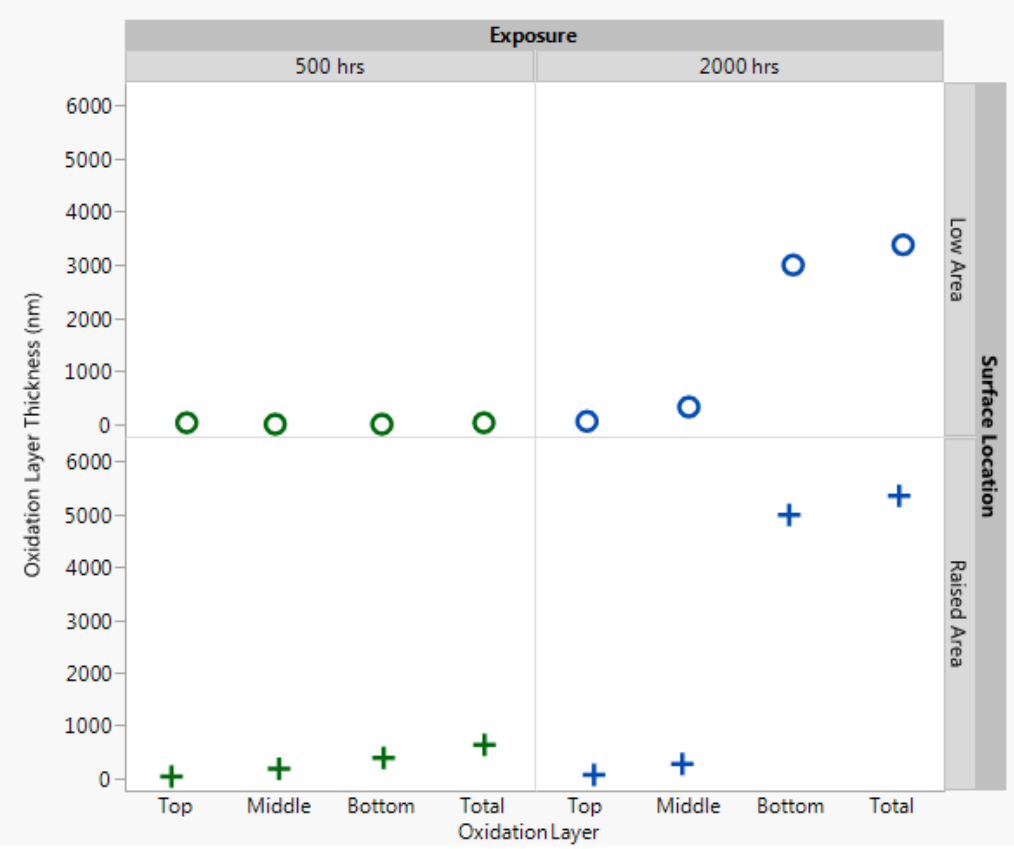

Fig. 11. Oxidation layer thickness changes from 500 to 2000 hours S-CO_2 exposure

3.3. Surface characterization

Information about corrosion product chemistry at sample surfaces was obtained by XPS. This has a very shallow probing depth (2-3 nm), and so this can provide the chemistry of the top-most layer on the samples. Fig. 12 shows the XPS spectra of the Fe 2p core level for both a 500 hr and 2000 hr sample. Here the Fe^{2+} and Fe^{3+} contributions are colored red and blue, respectively. The results indicate a contribution only from Fe^{3+} for both samples, with the contribution being stronger for the 2000 hr sample versus that for the 500 hr sample. From this analysis, it appears that the oxide layer on the outer surface of these samples is hematite (Fe_2O_3).

Raman spectroscopy, having a significantly deeper probing depth (> 1μm) than XPS, is able to provide chemistry information across the multiple oxide layers for these samples. Analysis for multiple areas of 500 hr and 2000 hr sample surfaces indicated the presence of both hematite (Fe_2O_3) as well as magnetite (Fe_3O_4) in each instance. X-ray diffraction of a 2000 hr sample surface further supports these results, as both hematite and magnetite peaks were present in the diffraction pattern. The XRD pattern for the 2000 hr sample is shown in Fig. 13. Collectively these analyses provide evidence that the oxidation layer consists of an outer hematite layer along with an inner magnetite layer.

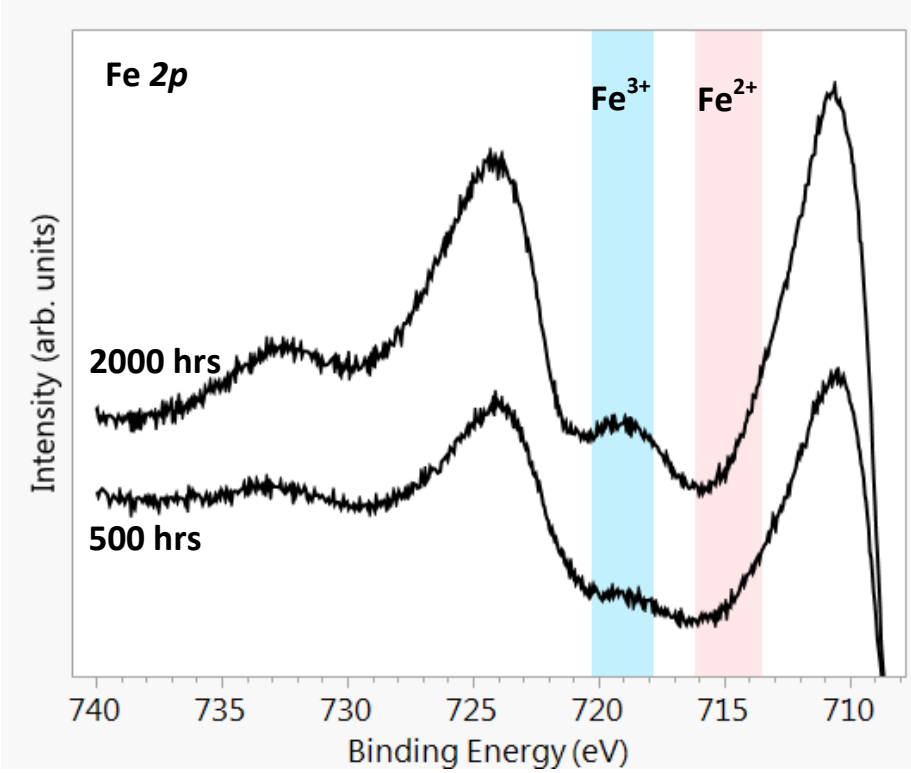

Fig. 12. Fe 2p photoelectron spectra obtained from sample surfaces at 500 and 2000 hrs exposure

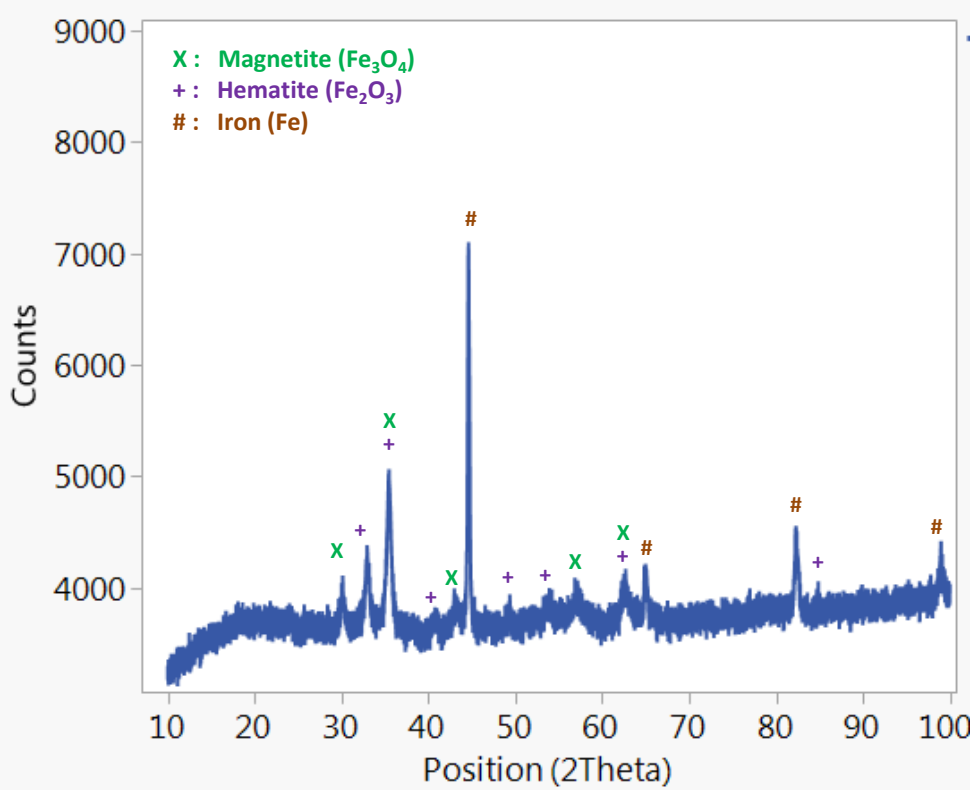

Fig. 13. Surface X-ray diffraction pattern for sample with 2000hrs S-CO_2 exposure

4. DISCUSSION

Corrosion measurements indicate the formation of an initially protective oxide scale after 1000 hrs exposure to the test conditions. At approximately 1500 hrs exposure, this scale loses its abililty to protect the base metal, resulting in faster linear breakaway oxidation at a rate of 0.032 mm/yr. Results similar to this have been described previously for carbon steel in CO_2 by Ferguson [4], whose schematic representation of breakaway corrosion is shown in Fig. 14.

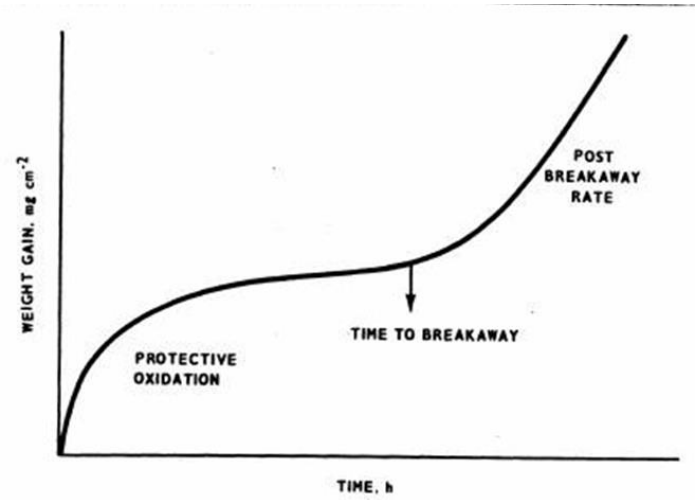

Fig. 14. Schematic representation of breakaway corrosion [4]

Microstructural characterization indicates the presence of cracks in the surface oxide layer at 2000 hrs exposure, whereas cracks are not obvious at shorter time intervals. Microstructural characterization also reveals the presence of multiple oxide layers on the samples, while surface analysis techniques identified the chemical phase for each of these layers. The outer-most oxide layer was identified as hematite (Fe_2O_3), while the oxide layer next to the base metal was shown to be magnetite (Fe_3O_4). Comparing the samples in Fig. 10, the rapid increase in total oxidation layer thickness from 500 to 2000 hours is dominated by growth of the inner magnetite layer.

Collectively, this information points to the transition from protective to breakaway oxidation caused by the formation of cracks in the surface hematite layer. A model was constructed by Gibbs[5] that describes this transition from protective to breakaway oxidation; this is shown in Fig. 15. Prior to the formation of these cracks, the growth rate of the oxidation layers is controlled by the rate of outward diffusion of Fe ions to the CO_2-oxide interface and the inward diffusion of vacancies to the oxide-metal interface. As the oxide thickness increases, the oxide scale becomes an effective barrier to Fe diffusion. Meanwhile, the accumulation of vacancies at the oxide-metal interface eventually reduces the mechanical integrity of this interface, to the point that cracks begin to form in the oxidation layers. Once these cracks form to a significant extent across the sample surface, they provide easier access of the base metal to CO_2. This results in an increase in the corrosion rate, as the rate of oxidation is no longer restricted by the rate of Fe outward diffusion and the inner oxide next to the base metal grows rapidly.

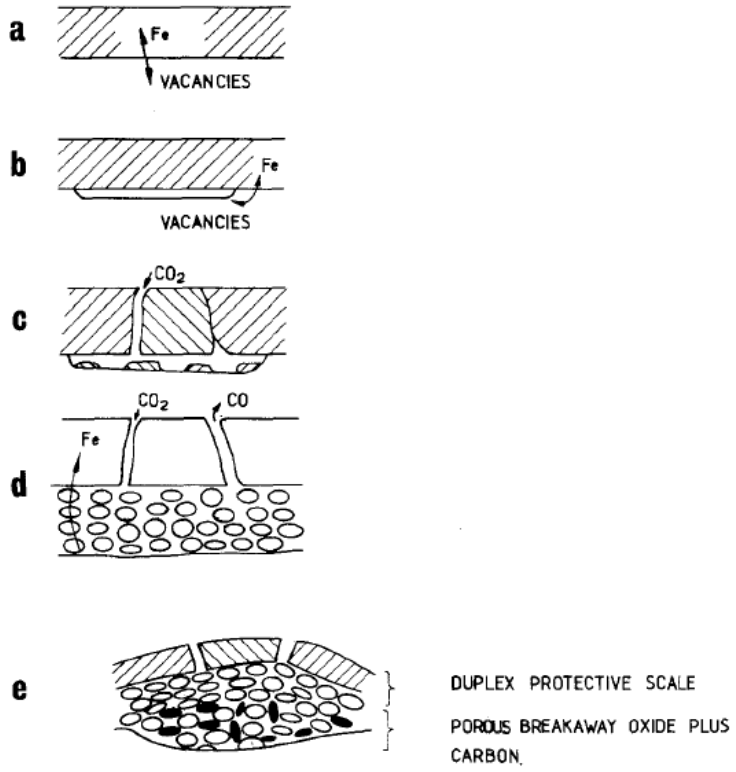

Fig. 15. Model for protective and breakaway oxidation of mild steel in CO_2 [5]

This model closely matches the observations from the samples in this work, with a two exceptions. One difference is the presence of both hematite and magnetite layers, whereas the model describes only magnetite. The reactions to form each of these phases are shown in equations (2) and (3). At the testing temperature both Fe_3O_4 and Fe_2O_3 are stable phases. The type and sequence of oxide layers which form depends on the partial pressure of oxygen. Naturally, the most oxygen-deficient oxide will reside next to the base metal and the most oxygen-rich oxide will be on the surface reacting with the gas phase. In the iron-oxygen system, the sequence from the innermost to outermost oxide layers will be Fe_3O_4 and Fe_2O_3. The presence of both oxides in these samples is reasonable. Their relative growth rates reflect the mechanisms for their reactions and how they shifts over time. The transition to breakaway oxidation and the resulting increase in magnetite growth can be explained by the improved pathways between the CO_2 and base metal.

$$3\,Fe + 4\,CO_2 = Fe_3O_4 + 4\,CO \quad (2)$$

$$2\,Fe + 3\,CO_2 = Fe_2O_3 + 3\,CO \quad (3)$$

The other difference is that the model describes the presence of significant carbon along with porosity in the inner oxide layer. The model explains this using the Boudouard reaction described in equation (4). It is unclear if this is the case for the samples from this test. While the microstructural analysis indicates the presence of porosity, analysis was not completed to understand the carbon concentration in this oxide layer.

$$2\,CO = CO_2 + C \quad (4)$$

Despite the transition to breakaway oxidation that was observed for these samples, the post-breakaway corrosion rate is rather small. The measured corrosion rate was used to estimate the time it will take to provide a 25% reduction in the starting thickness of the alloy. This is shown in Fig. 16 over a range of starting thicknesses. Predicted lifetimes based on this corrosion rate are very long, in excess of 50 years for each of the starting thicknesses.

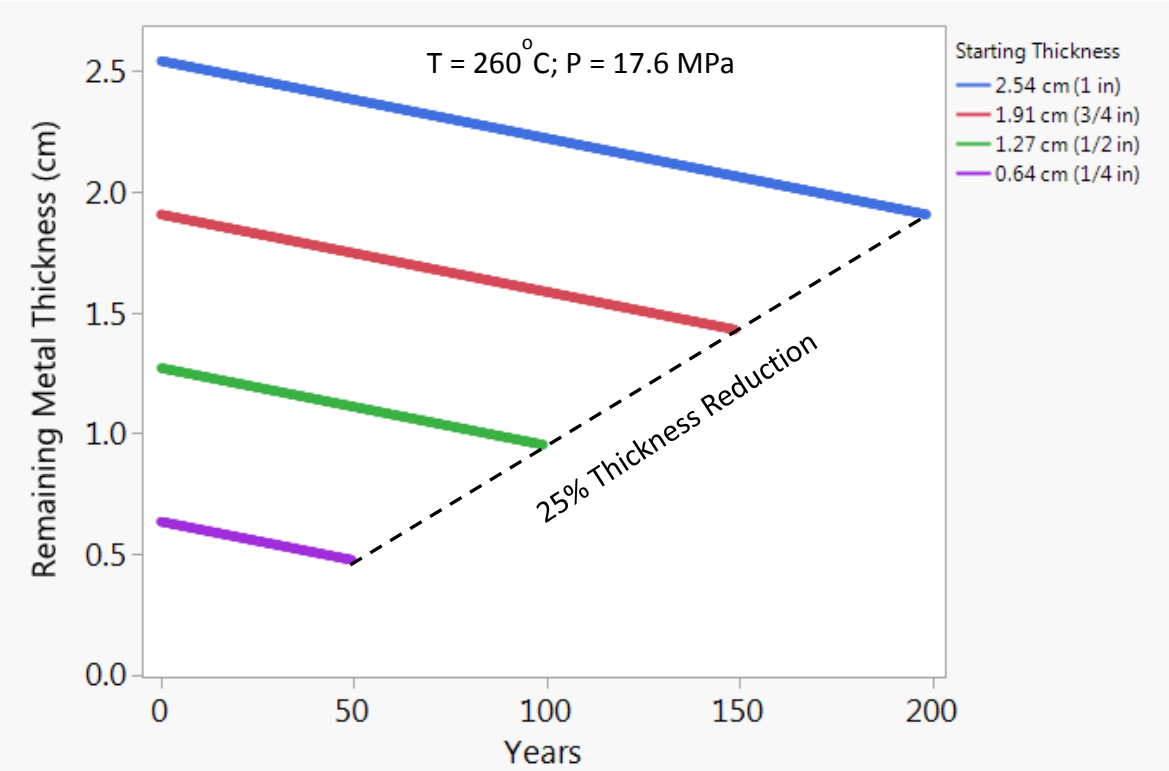

Fig. 16. Estimated times for a 25% reduction in alloy thickness using the post-breakaway corrosion rate

5. SUMMARY

Corrosion behavior of a carbon steel alloy (X65Q) was measured at 260°C and 17.6 MPa for up to 2000 hours S-CO_2 exposure. This inexpensive alloy is being explored as a replacement for more expensive stainless steel alloys in low to intermediate temperature portions of Sandia's closed Brayton loop. Corrosion was measured by two methods, both exhibiting the same behavior. The alloy forms an initial protective oxide scale, which after 1500 hours loses its ability to protect the base metal, resulting in breakaway oxidation with a measured corrosion rate of 0.032 mm/year. Transition to breakaway oxidation is attributed to cracks which form in the surface oxide, resulting in preferential growth of a thick magnetite (Fe_3O_4) layer beneath a hematite (Fe_2O_3) outer layer. Cracks in the hematite outer layer, enable CO_2 transport closer to the base metal surface, reducing the barrier (bulk Fe diffusion through the oxide scale) to the iron oxidation reaction. Despite the transition of the oxide scale from protective to breakaway after 1500 hours, the post-breakaway corrosion rate is still rather small. Predicted lifetimes based on this corrosion rate are very long, in excess of 50 years. While longer duration tests would certainly be prudent to understand if the oxide may spall after it grows thicker, based on the information from these tests, it appears that this alloy would suitable for use in Sandia's test loop.

NOMENCLATURE

S-CO_2 = Supercritical Carbon Dioxide
US DOE-NE = United States Department of Energy – Nuclear Energy Division
RCBC = Recompression Closed Brayton Cycle
CBC = Closed Brayton Cycle
MAGNOX = Magnesium Non-Oxidizing (Type of nuclear reactor designed in the UK)
AGR = Advanced Gas-cooled Reactor
HCl = Hydrochloric Acid
SEM = Scanning Electron Microscope
FIB = Focused Ion Beam
TEM = Transmission Electron Microscopy
STEM = Scanning Transition Electron Microscopy
HAADF = High-Angle-Annular-Dark-Field
XPS = X-ray Photoelectron Spectroscopy
XRD = X-ray Diffraction

ACKNOWLEDGEMENTS

Sandia National Laboratories is a multi-program laboratory managed and operated by Sandia Corporation, a wholly owned subsidiary of Lockheed Martin Corporation, for the U.S. Department of Energy's National Nuclear Security Administration under contract DE-AC04-94AL85000. SAND2016-0491C. Special acknowledgements to Farid El Gabaly Marquez for his contributions to this work through Raman and XPS Measurements. Also I would like to acknowledge Joshua Sugar and Suzy Vitale for their valuable contributions through FIB and STEM Analyses.

REFERENCES

1. Dostal, V., Driscoll, M. J., Hejzlar, P., *A Supercritical Carbon Dioxide Cycle for Next Generation Nuclear Reactors* (No. MIT-ANP-TR-100). Cambridge, MA: Massachusetts Institute of Technology, 2004.
2. Gibbs, J. P., Hejzlar, P., Driscoll, M. J., *Applicability of Supercritical CO_2 Power Conversion Systems to GEN IV Reactors* (No. MIT-GFR-TR-037). Cambridge, MA: Center for Advanced Nuclear Energy Systems – MIT Department of Nuclear Science and Engineering, 2006.
3. Choi, Y., Nesic, S., Corrosion Behavior of Carbon Steel in Supercritical CO_2-Water Environments, NACE Corrosion Conference, 2009.
4. Ferguson, J. M., Garrett, J., Lloyd, B., A Multivariate Investigation of the Kinetics of Oxidation of Mild Steels in High Temperature CO_2, British Nuclear Energy Society (BNES) Conference on Corrosion of Steels in CO_2, London, 1974.
5. Gibbs, G. B., A Model for Mild Steel Oxidation in CO_2, Oxidation of Metals, Vol. 7, No. 3, 1973, pp. 173-184.
6. Taylor, M. F., The Application of Thermodynamics to the Oxidation Behavior of Mild Steels in CO_2, Oxidation of Metals, Vol. 16, Nos. 1 / 2, 1981, pp. 133-146.
7. Brierley, R. A., Holmes, D. R., Studies of the Oxidation of 9 and 12Cr steels in high temperature, high pressure CO_2, British Nuclear Energy Society (BNES) Conference on Corrosion of Steels in CO_2, London, 1974.

8. Dewanckel, B., Leclercq, D., Dixmier, J., Holmes, D. R., Corrosion of Unalloyed or Low-Alloyed Steels in Pressurized CO_2, British Nuclear Energy Society (BNES) Conference on Corrosion of Steels in CO_2, London, 1974.
9. German, P. A., Litlejohn, A. C., Oxidation Kinetics of Carbon Steels in Pressurized CO_2-Based Atmospheres at Elevated Temperatures, , British Nuclear Energy Society (BNES) Conference on Corrosion of Steels in CO_2, London, 1974.
10. Propp, W. A., Corrosion in Supercritical Fluids, Idaho National Engineering Laboratory, INEL-96/0180, 1996.
11. American Society for Testing and Materials (ASTM). (2011). "Standard Practice for Preparing, Cleaning, and Evaluating Corrosion Test Specimens." *G1-03*, Philadelphia.
12. T. Degen, M. Sadki, E. Bron, U. König, G. Nénert; The HighScore Suite; Powder Diffraction / Volume 29 / Supplement S2 / December 2014, pp S13-S18.